



Environmentally-friendly 3D spherical catalysts derived from chitosan and oat for activation peroxyomonosulfate[☆]

Kewang Zheng^a, Zhen Tian^a, Yaoyao Zhang^a, Yuyang Du^a, Changchun Li^b, Lihang Shen^c, Wei Li^{a,*}, Caiqin Qin^{a,*}

^a School of Chemistry and Materials Science, Hubei Engineering University, Xiaogan, China

^b Hubei Key Laboratory of Quality Control of Characteristic Fruits and Vegetables, Hubei Engineering University, Xiaogan, China

^c Faculty of Engineering and Computing, The University of Sydney, Sydney, Australia

ARTICLE INFO

Editor: B. Van der Bruggen

Keywords:

Chitosan
Oats
Catalysts
Peroxyomonosulfate
Tetracycline

ABSTRACT

The demand for high-performance non-metallic catalytic materials that possess both exceptional decomposition efficiency and excellent separation capability is a significant challenge in the field of organic wastewater purification. In this work, the excellent cross-linking properties of chitosan (CS) and the rich starch content of oats were utilized to prepare environmentally-friendly 3D non-metallic spherical catalysts through a combination of freeze-drying and pyrolysis techniques. The incorporation of oats and urea effectively increased the specific surface area and the number of active sites of the catalysts, thereby enhancing their catalytic performance. When the mass ratio of chitosan to oats was 1:2 and the carbonization temperature was 700 °C, respectively, the spherical catalyst (CS@2Oat-N_U) exhibited excellent performance in activating PMS to degrade tetracycline (20 mg L⁻¹, 92.89 %). The CS@2Oat-N_U/PMS system involves both radical and non-radical pathways, with O₂^{•-} and ¹O₂ representing the primary ROSSs, and pyridine N, graphite N, C=O, and C-N groups serving as the predominant potential active sites. Cycling experiments and interference studies involving various anions confirmed the excellent stability and anti-interference properties of CS@2Oat-N_U. Furthermore, the favorable structural stability and adaptable dimensions of CS@2Oat-N_U render it an appropriate material for utilization as filtration components in flow-through reactors for wastewater treatment. The environmentally-friendly, exceptionally efficient, and easily separable 3D non-metallic spherical catalysts demonstrate potential for wastewater treatment.

1. Introduction

With the development of society and economy, antibiotics have been widely used in human life [1,2]. However, due to the limited absorption of antibiotics by organisms, a large amount of antibiotics is discharged into water bodies, causing serious water pollution [3,4]. Tetracycline is a typical broad-spectrum drug that was widely used in human medicine and animal husbandry [5]. However, tetracycline has a stable benzene ring structure, thus making it difficult for it to degrade on its own in the natural environment. The accumulation of tetracycline in water bodies can affect the ecological balance and threaten human health. Therefore, it is necessary to use effective measures to remove tetracycline from wastewater.

Currently, there are various techniques to degrade tetracycline, such

as adsorption, photocatalytic oxidation, and electrocatalytic oxidation [6–10]. Among them, advanced oxidation techniques based on peroxyomonosulfate are considered effective methods for wastewater treatment, due to their advantages of strong redox properties, fast reaction rate, and excellent stability [11]. However, PMS alone exhibits limited capability in generating reactive oxygen species (ROSSs) for pollutant degradation and demonstrates relative stability under normal conditions. To address this issue, carbon-based materials, UV light, and ultrasound are commonly used to activate PMS to generate reactive groups. However, there were certain disadvantages associated with these methods, such as the high energy consumption of UV light and secondary pollution caused by the leaching of transition metals [12,13]. Consequently, the development of efficient and environmentally friendly catalysts has emerged as a pivotal research area.

[☆] This article is part of a special issue entitled: 'Sustain energy & environ' published in Separation and Purification Technology.

* Corresponding authors.

E-mail addresses: weili@hbeu.edu.cn (W. Li), qincq@hbeu.edu.cn (C. Qin).

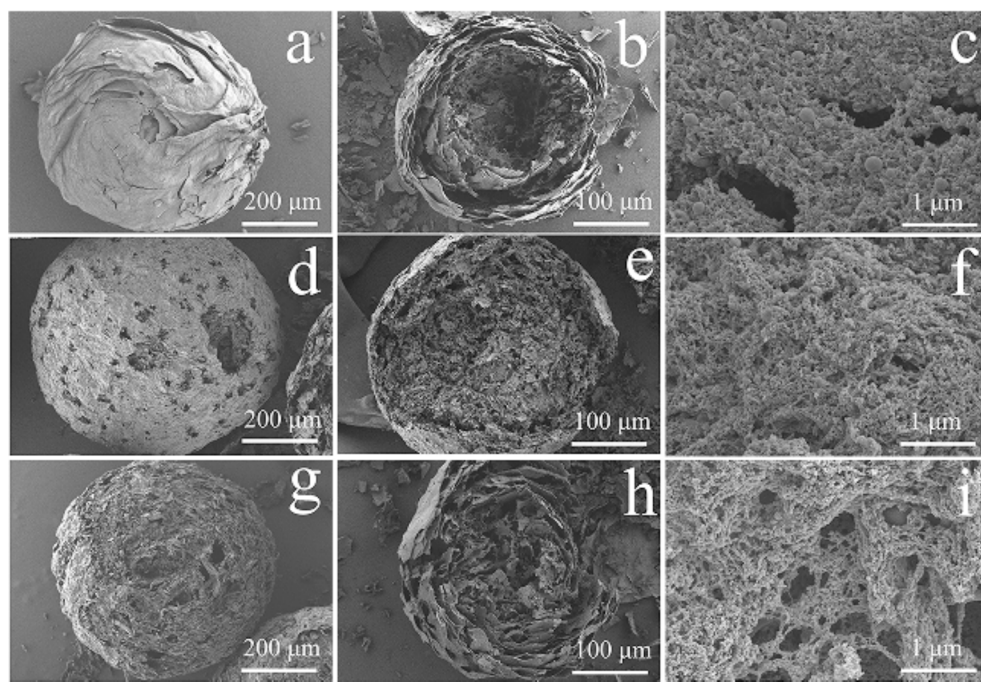


Fig. 1. SEM of C (a-c), CS@2Oat (d-f), CS@2Oat-N_U (g-i).

Carbon materials derived from biomass have garnered increasing attention as a prominent catalyst material in recent years, owing to their metal-free leaching properties and favorable activation activity towards PMS [14–16]. Oats represent the sixth largest grain crop, with an extensive global cultivation area [17]. The principal constituents of oats are starch, protein, fiber, lipids, and a small quantity of minerals, which exert an influence on the structure and properties of composite materials [18–21]. However, due to improper transportation and storage, a large amount of oats become moldy every year and produce excessive levels of aflatoxin, resulting in the waste of these oat resources. Therefore, how to effectively and fully utilize these moldy oats is crucial for agricultural development and environmental protection.

Chitosan (CS) is a product of deacetylation of chitin, which had the advantages of non-toxicity, biocompatibility, and biodegradability [22]. Additionally, CS was rich in hydroxyl and amino groups, which could be modified by cross-linking and graft copolymerization to obtain related derivatives [23]. However, the activation of PMS for antibiotic degradation by 3D porous carbon spheres prepared from oats and CS has not been reported yet. Therefore, since oats are a cheap, abundant, and renewable biomass resource, 3D porous microspheres could be prepared using oats as the supporting skeleton, chitosan as the catalyst carrier, and sodium tripolyphosphate as the cross-linking agent for the activation of PMS for the efficient degradation of TC.

In this paper, 3D porous spherical carbon-based catalysts derived from oat and CS were prepared for the activation of PMS to degrade TC. The effects of oat content and nitrogen sources on the structure and degradation performance of the catalysts were investigated. The catalysts' structures were characterized by scanning electron microscopy (SEM), Raman spectroscopy, and pore structure analysis. The impacts of various environmental factors on degradation performance were examined. Additionally, the mechanism of the catalyst/PMS/TC system was explored through electron paramagnetic resonance (EPR), high performance liquid chromatography-mass spectrometry (HPLC-MS), scavenging experiments, and electrochemical tests.

2. Material and methods

2.1. Material

The materials were shown in [Supporting Information](#) (Text S1).

2.2. Catalyst synthesis

2 g of crushed oats and 2 g of a nitrogen source were simultaneously added to 100 mL of a 2 % chitosan (CS) solution, which was then stirred at high speed for 5–10 min to obtain a well-dispersed mixed viscous liquid. The above mixture was subsequently transferred to a syringe and slowly dripped into a 1 % sodium tripolyphosphate aqueous solution for cross-linking to form spherical structures. After 12 h of static incubation, the spheres were washed several times with deionized water and ethanol, followed by freeze-drying to obtain the precursor spheres. Finally, the precursor was heated to 700 °C for 3 h at a heating rate of 5 °C min⁻¹ under N₂ protection to obtain the catalyst. The effects of oat content and nitrogen source on the catalytic performance were investigated. Samples named CS@xOat-N_y, where x represents the mass ratio of oat to CS (x = 1, 2, and 3), and y denotes the type of nitrogen source (urea-U, dicyandiamide-D, melamine-M, and thiourea-T). Additionally, samples labeled C (without oat and urea) were prepared by a similar method.

2.3. Characterizations

Detailed catalytic and analytic methods can be found in [Supporting Information](#) (Text S2).

3. Results and discussion

3.1. Characterization

The morphology of the catalysts was characterized by means of SEM. As shown in [Fig. 1](#), all the samples display a regular spherical structure with comparable dimensions. However, notable discrepancies are evident in their surface and internal pore structures. In detail, the

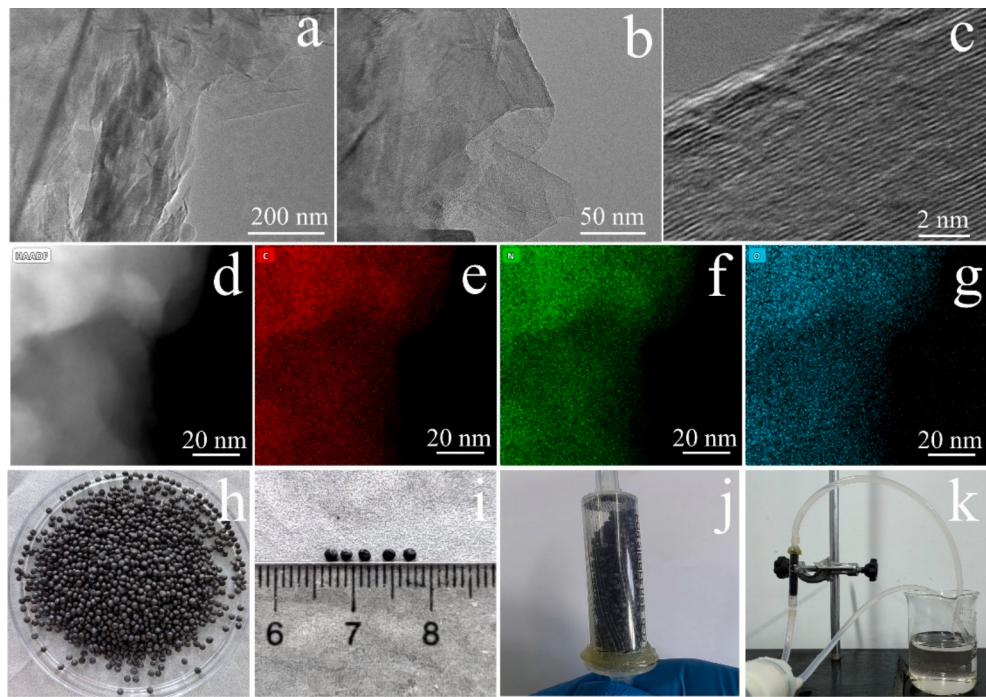


Fig. 2. TEM (a-c), elemental mapping (d-g) and digital photos (h-k) of CS@2Oat-N_U.

surface of the spheres of pure C is notably smooth and intact, with the vast majority of pore channels effectively covered by the carbon layer, and its interior exhibits a continuous lamellar hollow structure, which may be due to the cross-linking of CS and sodium tripolyphosphate exclusively at the surface (Fig. 1a-c). When oats were incorporated, the complete covering of the CS@2Oat surface was disrupted, resulting in the exposure of portions of the pore channel (Fig. 1d-f). Concurrently, the interior of the structure became filled. The simultaneous addition of oats and urea resulted in further alterations of the structure of CS@2Oat-N_U. The surface of CS@2Oat-N_U became increasingly irregular and porous, and its interior also exhibited an irregular, scale-like porous structure, but no hollow structure was observed (Fig. 1g-i). This phenomenon can be attributed to the synergistic effect of oats and urea. Firstly, the presence of oats can act as a supporting skeleton, which reduces the coverage of the catalyst surface by the carbon layer formed during the cross-linking process, thereby improving the exposure rate of the catalyst active sites. Secondly, the presence of urea not only provides abundant nitrogen for the catalyst but also generates a large number of volatile gases during the pyrolysis process. This produces a pore-expanding effect on the catalyst from the inside out, increasing the specific surface area and pore size of the catalyst. These observations collectively indicate that both oat and urea doping contribute to the formation of the porous structure of the catalyst. This porous structure

may potentially reduce mass transfer resistance and enhance the catalytic performance [24,25].

To further analyze the microstructure of CS@2Oat-N_U, TEM was used for characterization. As shown in Fig. 2a and 2b, TEM revealed a layered structure similar to that observed in SEM. High-resolution TEM (Fig. 2c) showed numerous ordered carbon layers, with a calculated lattice spacing of 0.328 nm, indicating the presence of graphite-like carbon structures in the sample. The elemental distribution of CS@2Oat-N_U was investigated using HAADF-STEM and elemental mapping. The results demonstrated that the C, N, and O elements were distributed uniformly throughout the catalyst. Furthermore, the digital images of CS@2Oat-N_U were captured. As depicted in Fig. 2h and 2i, these carbon spheres exhibit uniform spherical morphology with particle sizes ranging from approximately 1 to 1.5 mm. This observation highlights their potential application as fillers in wastewater filters for continuous and efficient treatment of wastewater (Fig. 2j and 2k).

The crystal structures of the catalysts were characterized by X-ray diffraction (XRD). As shown in Fig. 3a, all the samples showed a distinct characteristic peak near 26.4°, which is attributed to the (002) plane of graphitic carbon [26]. Furthermore, the relative peak intensity of CS@2Oat-N_U is markedly higher than that of C and CS@2Oat, suggesting that CS@2Oat-N_U contains a greater proportion of graphitic carbon. This phenomenon can be attributed to the fact that the thermal

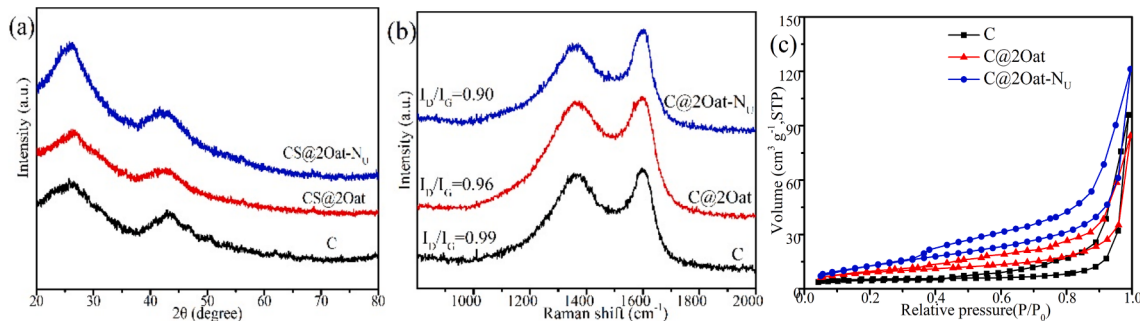


Fig. 3. XRD patterns (a), Raman spectra (b), N₂ adsorption–desorption isotherms (c).

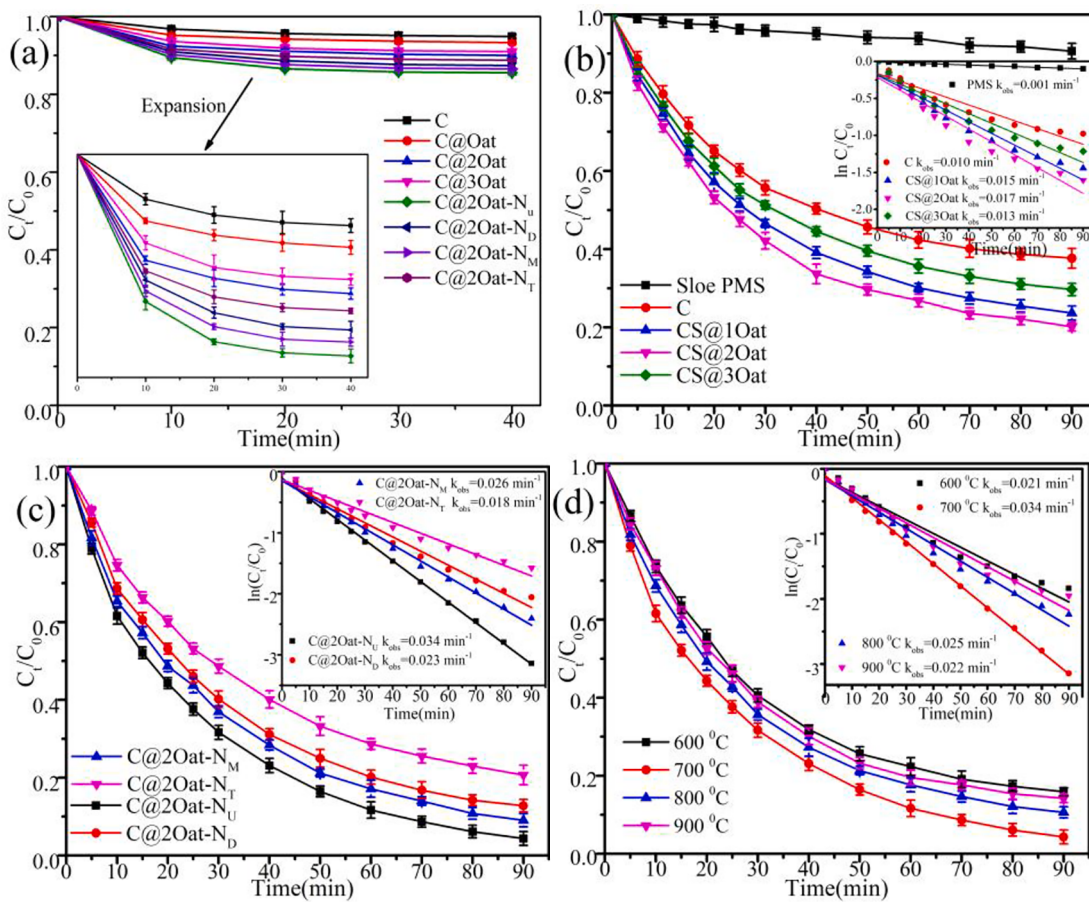


Fig. 4. Effect of different catalyst on adsorption performance (a). Effect of oat dosage (b), nitrogen source (c), and pyrolysis temperature (d) on degradation performance. Conditions: $[TC]_0 = 20 \text{ mg L}^{-1}$, $[\text{catalyst}]_0 = 0.20 \text{ g L}^{-1}$, $[\text{PMS}]_0 = 0.20 \text{ g L}^{-1}$, pH = 3.68, T = 25 °C.

decomposition of urea promotes the transformation of amorphous carbon into graphitic carbon under high-temperature conditions, thus increasing the percentage of graphitic carbon.

The graphitization degree of the catalyst is determined by Raman spectroscopy. The graphitization degree of catalysts was usually measured by the ratio of D and G band peak heights (I_D/I_G), with higher ratios indicating a lower graphitization degree in the samples [27]. As illustrated in Fig. 3b, all samples exhibited characteristic peaks around 1345 cm^{-1} and 1575 cm^{-1} , which correspond to amorphous carbon and graphitic carbon, respectively. The I_D/I_G ratios for C, CS@2Oat, and CS@2Oat-N_U were 0.99, 0.96, and 0.9, respectively, suggesting that CS@2Oat-N_U forms more graphitized structures.

The structural characteristics of C, CS@2Oat, and CS@2Oat-N_U catalysts were determined by N_2 adsorption–desorption isotherms. As illustrated in Fig. 3c, all catalysts displayed the characteristics of a type IV isotherm, accompanied by the presence of adsorption hysteresis loops. This observation suggests that the samples possess a mesoporous structure. As depicted in Table S1, the S_{BET} , average pore size and pore volume of CS@2Oat-N_U ($124.56 \text{ m}^2 \text{ g}^{-1}$, 7.54 nm , $0.059 \text{ cm}^3 \text{ g}^{-1}$) were higher than those of CS@2Oat ($85.65 \text{ m}^2 \text{ g}^{-1}$, 6.54 nm , $0.045 \text{ cm}^3 \text{ g}^{-1}$) and C ($62.98 \text{ m}^2 \text{ g}^{-1}$, 4.62 nm , $0.033 \text{ cm}^3 \text{ g}^{-1}$), indicating that the incorporation of urea and moderate quantities of oats is advantageous in enhancing the pore structure of the catalyst. This is because urea can generate a substantial quantity of volatile gas during pyrolysis, which leads to the expansion of the pores in the carbon spheres. The addition of oats can further enhance this effect by reducing the density of the carbon spheres and improving the dispersion of urea. The results demonstrate that CS@2Oat-N_U exhibits a high specific surface area, average pore diameter, and pore volume, which collectively provide a substantial

number of active sites to enhance the activation performance of PMS [28].

3.2. Evaluation of catalyst performance

The performance of the prepared catalysts for TC degradation was determined using the PMS activation method. As illustrated in Fig. 4a, the adsorption percentages of all samples within 40 min were relatively low (less than 20 %), which could be attributed to an inadequate contact area between the catalyst and TC. Nevertheless, the CS@2Oat-N_U exhibits the highest adsorption percentage, which may be attributed to its larger surface area and pore size. As illustrated in Fig. 4b, the degradation percentage of TC (20 mg L^{-1}) by PMS alone reached only 9.4 % and an apparent rate constant (k_{obs}) of 0.001 min^{-1} within 90 min, indicating that PMS alone has a weak ability to oxidize TC. It was also found that the degradation percentage and k_{obs} of TC initially increased and then decreased as the doping amount of oats varied. When the mass ratio of oats to CS was 2, the degradation percentage and k_{obs} reached the highest values of 79.88 % and 0.017 min^{-1} , respectively, which might be attributed to the provision of additional active sites for the activation of PMS and generating ROSs. When the mass ratio of oats to CS was 1, the higher concentration of sodium tripolyphosphate reacted with CS to form hollow spheres with a denser surface structure. This inhibited the effective reaction between the catalyst, PMS, and TC, resulting in a suboptimal degradation efficiency of TC. At the mass ratio of 3, the higher amount of oats resulted in a higher density of the catalyst, thus reducing the number of spheres in the reaction system, which also inhibited the reaction between the catalyst, PMS, and TC. Therefore, the optimal mass ratio of oats to CS was 2.

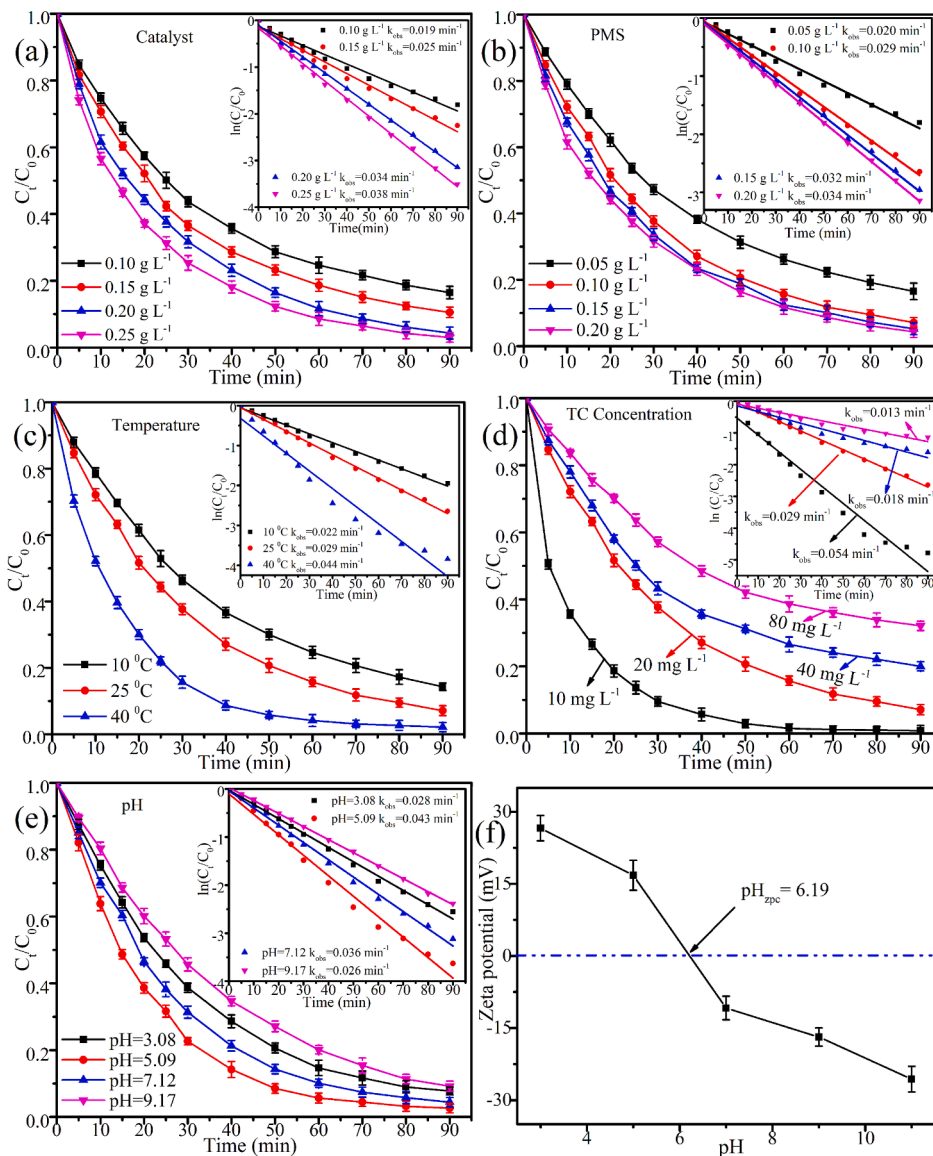


Fig. 5. Effect of catalyst dosages (a), PMS dosages (b), temperature (c), TC concentration (d), initial pH (e) on degradation process. Effect of pH on zeta potential (f). Conditions: $[TC]_0 = 20 \text{ mg L}^{-1}$, $[CS@2Oat-N_U]_0 = 0.20 \text{ g L}^{-1}$, $[PMS]_0 = 0.10 \text{ g L}^{-1}$, $pH = 3.68$, $T = 25^\circ\text{C}$.

The impact of doping disparate nitrogen sources on the catalytic performance of the catalyst is illustrated in Fig. 4c. When urea was added, the degradation percentage and k_{obs} increased to 95.68 % and 0.034 min⁻¹, respectively. This observation can be attributed to the potential of N atoms to modulate the electronic configuration of the carbon network, thereby facilitating electron transfer and the formation of ROSS [29]. The addition of urea exhibited the most effective degradation performance comparison to other nitrogen sources. This can be attributed to the fact that urea is soluble in water and can be more effectively dispersed in the catalyst.

Fig. 4d illustrates that the degradation efficiency of TC increased from 84.11 % to 95.68 % as the calcination temperature increased from 600 °C to 700 °C. This phenomenon could be attributed to the formation of graphitic carbon and graphitic nitrogen at a suitable calcination temperature [30]. Nevertheless, the degradation percentage of TC decreased to 89.35 % and 85.79 % with the calcination temperature increased to 800 °C and 900°C, respectively. This may be attributed to the collapse of the porous structure of the catalyst and the reduction in the number of active sites. Therefore, the optimal calcination temperature is 700 °C. Based on the above data, the CS@2Oat-N_U was used for

the following part.

The impact of catalyst dosage on the degradation performance of TC is shown in Fig. 5a. As the catalyst dosage increased from 0.10 g L⁻¹ to 0.20 g L⁻¹, the degradation efficiency of TC exhibited a notable rise, reaching 95.68 % from 83.55 %. Concurrently, the k_{obs} value augmented from 0.019 min⁻¹ to 0.034 min⁻¹. This phenomenon may be attributed to the fact that a higher catalyst dosage provides a greater number of active sites [31]. Upon increasing the dosage of the catalyst to 0.25 g L⁻¹, the degradation percentage and k_{obs} of TC only increased to 96.99 % and 0.038 min⁻¹, respectively. Accordingly, the optimal dosage of the catalyst was established as 0.2 g L⁻¹ based on both degradation performance and economic viability.

The effect of PMS dosage on TC degradation was investigated in Fig. 5b. The findings demonstrated that TC degradation efficiency could reach 83.48 % when the PMS dosage was 0.05 g L⁻¹, thereby indicating that the catalyst exhibited an exemplary catalytic capacity for TC. An increase in the dosage of PMS from 0.05 g L⁻¹ to 0.10 g L⁻¹ resulted in a corresponding increase in the degradation efficiency and k_{obs} of TC from 83.48 % and 0.02 min⁻¹ to 92.89 % and 0.029 min⁻¹, respectively. This phenomenon indicated that an appropriate increase in the dosage of

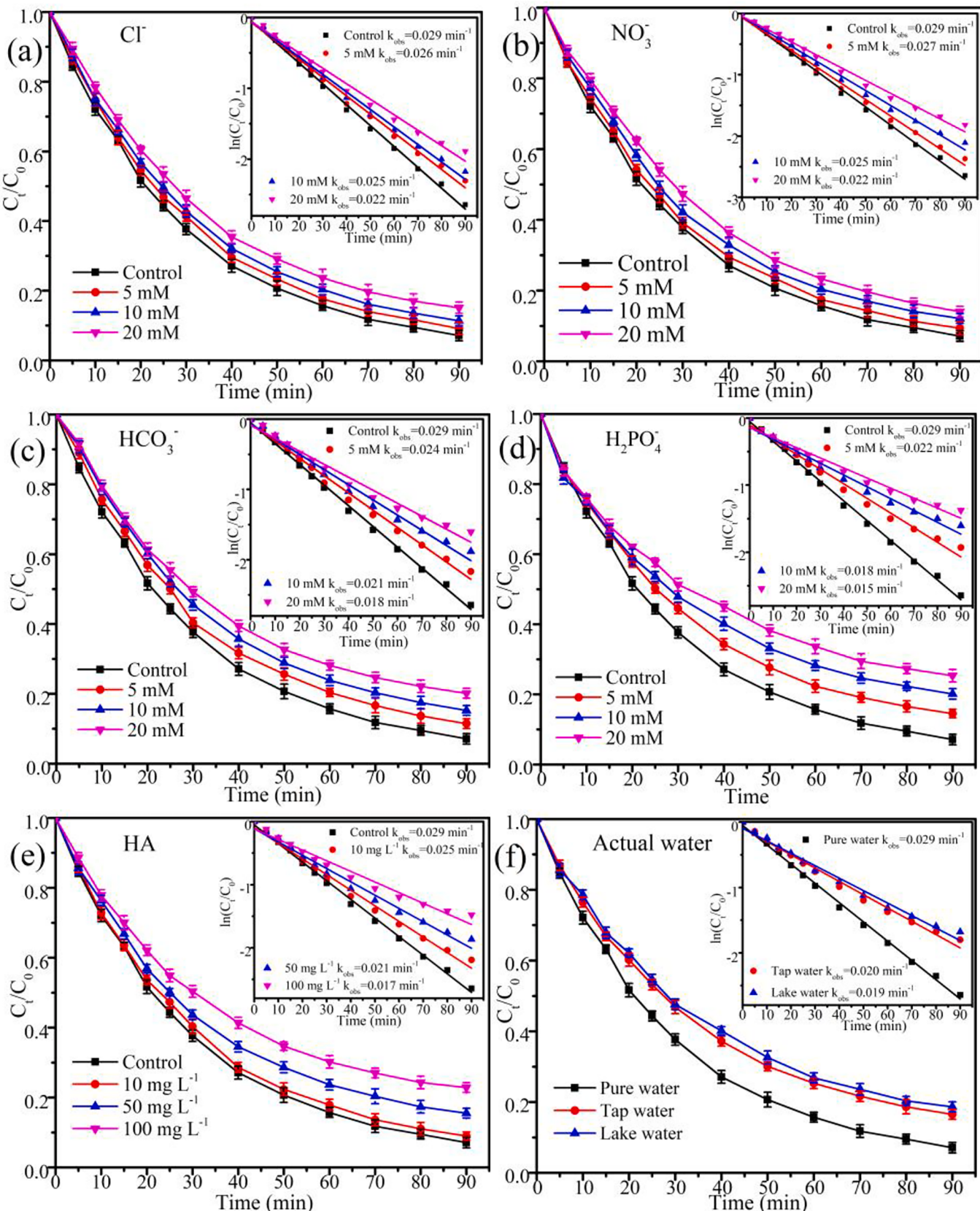


Fig. 6. Different water conditions. Conditions: $[\text{TC}]_0 = 20 \text{ mg L}^{-1}$, $[\text{CS@2Oat-Nu}]_0 = 0.20 \text{ g L}^{-1}$, $[\text{PMS}]_0 = 0.10 \text{ g L}^{-1}$, pH = 3.68, T = 25 °C.

PMS could result in the production of a greater number of ROSSs for TC degradation [32]. Nevertheless, when the PMS concentration was further increased to 0.15 g L⁻¹ and 0.2 g L⁻¹, no significant impact was observed on the ultimate degradation efficiency of TC. This is probably because excessive use of PMS can lead to self-consuming reactions, thereby weakening the degradation process. Accordingly, the optimal PMS dosage in the CS@2Oat-N_U/PMS system was determined to be 0.10 g L⁻¹. Moreover, to further evaluate the catalytic activity of CS@2Oat-N_U, a comparison was conducted between the performance of CS@2Oat-N_U in activating PMS for the degradation of TC and that reported in previous studies. The corresponding data are shown in Table S2, which demonstrates that despite the low concentration of both the catalyst and PMS in the CS@2Oat-N_U/PMS system, its degradation efficiency of TC remains high, indicating the remarkable efficacy of the CS@2Oat-N_U/PMS system in removing antibiotics from water.

The environmental water temperature displays significant variability due to the influence of diverse regional and seasonal conditions. Consequently, it is of paramount importance to investigate the influence of reaction temperature on the degradation performance [33]. As illustrated in Fig. 5c, the degradation efficiency and k_{obs} of TC exhibited a notable enhancement from 85.68 % and 0.022 min⁻¹ to 97.85 % and 0.044 min⁻¹ as the reaction temperature increased from 10 °C to 40 °C. This observation suggests that higher reaction temperatures are conducive to the activation of PMS and the generation of a greater number of ROSSs, which promote the degradation reaction. Additionally, the apparent activation energy (E_a) of CS@2Oat-N_U was determined using the Arrhenius equation, and it was calculated to be 17.35 kJ mol⁻¹, indicating that the CS@2Oat-N_U has satisfactory catalytic activity.

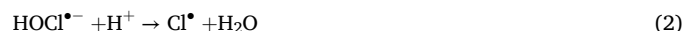
As illustrated in Fig. 5d, the effect of initial TC concentration on degradation performance was determined. It was observed that the degradation percentage exhibited a gradual decline as the initial TC concentration increased from 10 mg L⁻¹ to 80 mg L⁻¹. As the concentration of TC increased, the concentration difference between TC and ROSSs gradually increased, leading to enhanced competitive adsorption of PMS and TC onto the catalyst [34]. Additionally, a higher initial TC concentration necessitates a longer reaction time to achieve equivalent degradation efficiency. This phenomenon can be attributed to the competitive consumption of ROSSs by intermediates generated within the reaction system. Upon reaching an initial TC concentration of 80 mg L⁻¹, the final degradation efficiency remained at 67.88 %, which further substantiates the exceptional PMS activation performance of the catalyst.

The impact of pH on the degradation performance of TC is presented in Fig. 5e. As the pH of the solution increased from 3.08 to 5.09, the degradation efficiency and k_{obs} of TC increased from 92.22 % and 0.028 min⁻¹ to 97.35 % and 0.043 min⁻¹, respectively. Nevertheless, further increases in pH to 7.12 and 9.17 resulted in a decline in both the degradation efficiency and k_{obs} of TC. To determine the zeta potential of CS@2Oat-N_U under different pH conditions, measurements were taken, and the results are presented in Fig. 5f. The estimated isoelectric point (pH) is approximately 6.19, indicating that the surface charge of CS@2Oat-N_U is positive when pH < 6.19 and negative when pH > 6.19. In addition, research has shown that the dissociation constants (pKa) of TC are 3.32, 7.78, and 9.58, respectively [35,36]. When the pH is less than 3.32, TC exists in cationic form (TC₃⁺); when the pH is between 3.32 and 7.78, TC exists in zwitterionic form (TC₂[±]); while the pH is greater than 7.78, TC exists in anionic form (TC⁻ or TC²⁻). When the solution pH is 3.08, there is a strong electrostatic repulsion between protonated TC and positively charged CS@2Oat-N_U, which hinders the adsorption of TC on the catalyst surface. However, a lower pH is beneficial for improving the positive charge on the catalyst surface and promoting mass transfer between the catalyst and PMS molecules. When the pH is 5.09 and 7.12, there is no electrostatic repulsion between the zwitterionic form of DTC molecules and the catalyst; however, at a pH of 5.09, the positive charge on the catalyst surface is higher than that at a

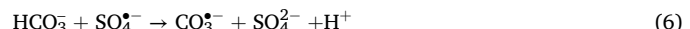
pH of 7.12, which is more favorable for the activation of PMS molecules. Therefore, the degradation effect is optimal at a pH of 5.09. Conversely, at a pH of 9.17, a robust electrostatic repulsion between the anionic form of TC and the negatively charged catalyst not only impedes the adsorption of DTC molecules on the catalyst surface but also contributes to the conversion of HSO₅⁻ to the less reactive SO₅²⁻ under alkaline conditions [37]. This ultimately results in a reduction in TC removal efficiency and reaction rate.

3.3. Co-existing compounds

To assess the catalytic performance of CS@2Oat-N_U in different environments, the degradation experiments were measured in the presence of various inorganic anions (NO₃⁻, HCO₃⁻, HPO₄²⁻, Cl⁻) and natural organics (humic acid), as illustrated in Fig. 6. The presence of Cl⁻ and NO₃⁻ has been observed to exert a slight inhibitory effect on the degradation reaction, with a concomitant decrease in the degradation percentage and k_{obs} of TC. Specifically, at concentrations of 20 mM for Cl⁻ and NO₃⁻, the degradation percentage and k_{obs} of TC decreased from 92.89 % and 0.029 min⁻¹ (control) to 84.88 %, 0.022 min⁻¹ (Cl⁻) and 85.99 %, 0.022 min⁻¹ (NO₃⁻), respectively (Fig. 6a and 6b). This phenomenon might be attributed to the tendency of Cl⁻ and NO₃⁻ to react with SO₄²⁻ and •OH, forming Cl[•], Cl₂^{•-} and NO₃[•], which have weak redox capacity, thus inhibiting the degradation of TC [38].



As illustrated in Fig. 6c and 6d, the presence of HCO₃⁻ and H₂PO₄⁻ also resulted in a mild inhibition of the degradation reaction. When the concentration of HCO₃⁻ and H₂PO₄⁻ was 20 mM, the degradation efficiency and k_{obs} of TC exhibited a decline from 92.89 % and 0.029 min⁻¹ (control) to 79.88 %, 0.018 min⁻¹ (HCO₃⁻) and 75.68 %, 0.015 min⁻¹ (H₂PO₄⁻), respectively, which could be caused by several factors. Firstly, the addition of HCO₃⁻ and H₂PO₄⁻ increased the pH of the reaction solution to 8.7 and 9.01, respectively, altering the surface charge of the catalyst and weakening its adsorption of TC molecules. Secondly H₂PO₄⁻ can quench SO₄²⁻ and •OH, while HCO₃⁻ can react with ROSSs to produce HCO₃⁻ with a lower redox potential [39]. Lastly HCO₃⁻ and H₂PO₄⁻ can be adsorbed on the catalyst surface, thus reducing the contact of PMS and TC molecules with the catalyst's active sites.



As depicted in Fig. 6e, the degradation reaction was negligibly influenced by the low concentration of HA. This was attributed to the adsorption of TC molecules by HA, which resulted in a slight reduction in TC concentration within the solution. However, when the HA concentration reached 100 mg L⁻¹, a notable inhibition in the degradation process was observed, with the final degradation percentage and k_{obs} of TC being only 77.14 % and 0.017 min⁻¹, respectively. This was attributed to the fact that the increase in HA concentration led to greater adsorption of HA on the catalyst surface, which in turn impeded the interaction between the catalyst's active sites and the PMS molecules, thereby inhibiting the degradation of TC [40].

In addition, the effects of different actual waters on TC degradation were also investigated. As shown in Fig. 6f, the degradation efficiency and k_{obs} of TC in tap water and lake water decreased to 83.48 %, 0.02

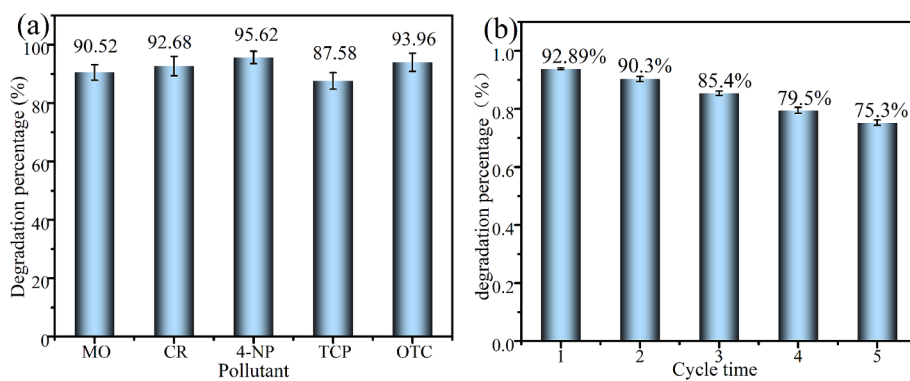


Fig. 7. Different organic pollutants (a), Cycles times (b). Conditions: $[{\text{pollutant}}]_0 = 20 \text{ mg L}^{-1}$, $[\text{CS@2Oat-N}_U]_0 = 0.20 \text{ g L}^{-1}$, $[\text{PMS}]_0 = 0.10 \text{ g L}^{-1}$, pH = 3.68, T = 25 °C.

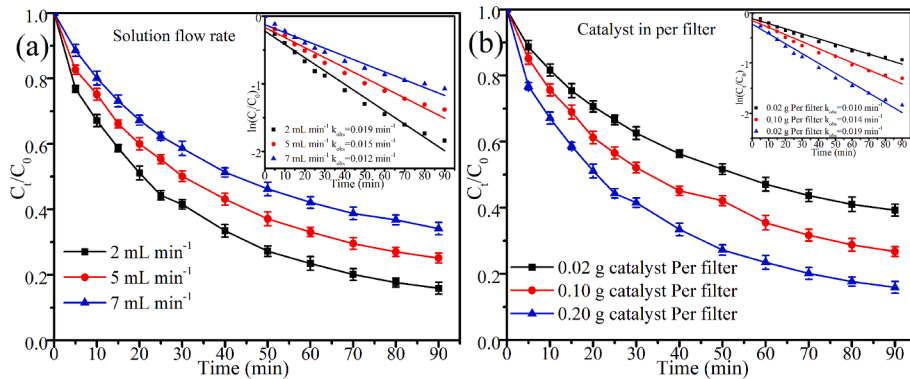


Fig. 8. Solution flow rate (a) and catalyst amount in per filter on dynamic flow degradation. Conditions: $[\text{TC}]_0 = 20 \text{ mg L}^{-1}$, $[\text{PMS}]_0 = 0.10 \text{ g L}^{-1}$, pH = 3.68, T = 25 °C.

min^{-1} and 83.15 %, 0.019 min^{-1} , respectively. By analyzing the parameters such as the hardness of lake water and tap water (Table S3), it was found that the inhibition of the degradation efficiency was mainly due to the presence of higher concentrations of HCO_3^- in both lake water and tap water. The above results indicate that CS@2Oat-N_U exhibits excellent environmental adaptability.

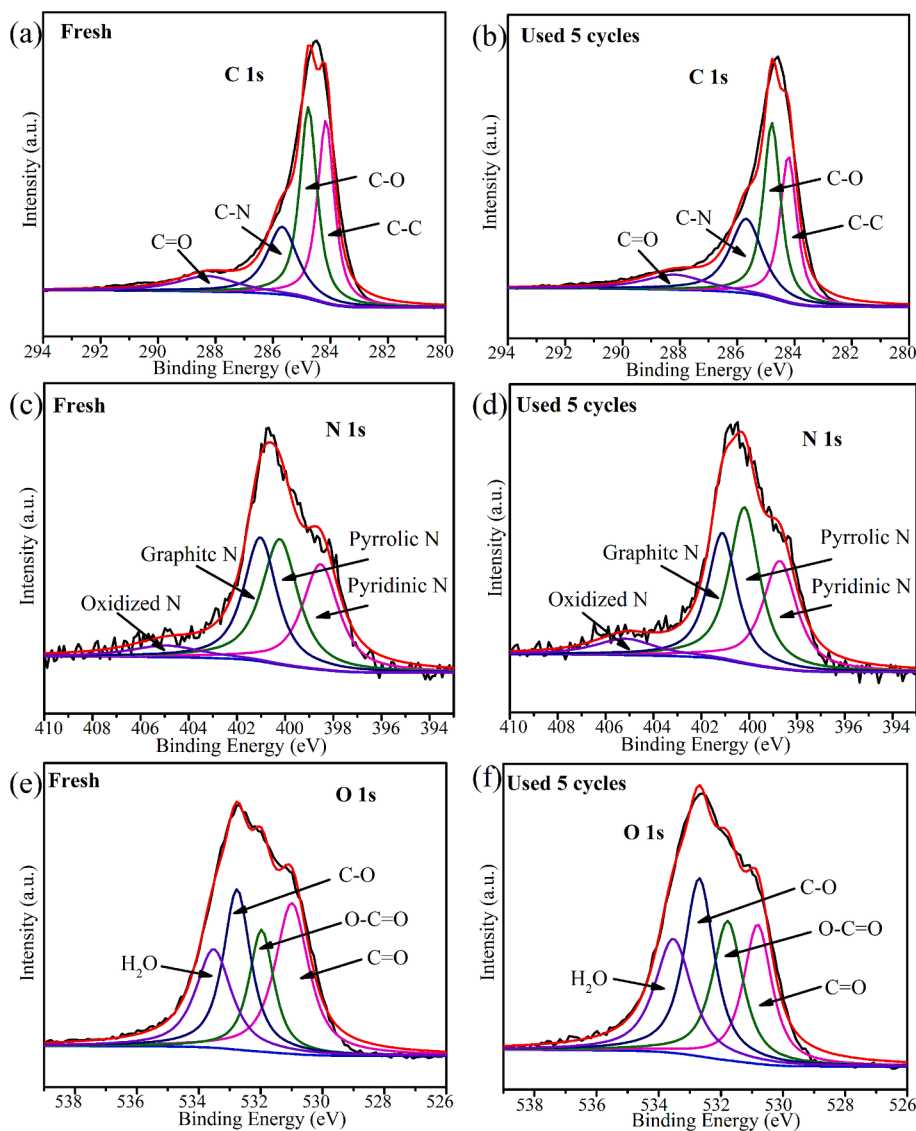
3.4. Recyclability and stability of catalyst

The extensive applicability of the catalyst on different pollutants was investigated by activating PMS for the degradation of trichlorophenol (TCP), methyl orange (MO), Congo red (CR), oxytetracycline (OTC) and 4-nitrophenol (4-NP). As illustrated in Fig. 7a, the degradation percentages of 20 mg L⁻¹ MO, CR, 4-NP, TCP, and OTC reached 90.52 %, 92.68 %, 95.62 %, 87.58 %, and 93.96 %, respectively. The result demonstrated that the prepared CS@2Oat-N_U exhibits satisfactory universality.

To investigate the stability and reusability of the catalyst, cyclic degradation experiments were carried out. As illustrated in Fig. 7b, the catalyst demonstrated sustained high degradation performance after five cycles, with the degradation percentage decreasing only from 92.89 % to 75.3 %, indicating that CS@2Oat-N_U had good stability for the degradation of organic pollutants by activated PMS. The decline in degradation efficiency could be attributed to oxidation and accumulation of impurities on the catalyst surface. Furthermore, after five cycles of reuse, the catalyst maintained a complete spherical structure, with no evidence of component shedding or material decomposition. These findings demonstrate the mechanical strength of CS@2Oat-N_U and its suitability for practical applications.

3.5. Evaluation of dynamic flow degradation

The dynamic flow continuous degradation performance of the catalyst was evaluated under different solution flow rates using a filter containing varying amounts of CS@2Oat-N_U, which was used to single-pass catalytically oxidize TC. The experimental setup is illustrated in Fig. 2k. A single cycle of catalytic oxidation was complete as the solution in one beaker was fully filtered into another beaker. As shown in Fig. 8a, the degradation percentage of TC gradually decreased as the solution flow rate increased. This phenomenon can be attributed to the fact that increasing the solution flow rate not only reduces the contact and residence time between TC, PMS, and the catalyst. Additionally, the impact intensity resulting from the augmented flow rate is not conducive to the adsorption of TC and PMS molecules on the catalyst surface. When the solution flow rate was 2, 5, and 7 mL min^{-1} , the TC degradation percentage reached 84.12 %, 74.88 %, and 65.88 %, respectively. Since the amount of catalyst in the filter has an important effect on the activation of PMS molecules as well as the adsorption of TC molecules, the effect of the catalyst amount in the filter on the degradation of TC was investigated. Fig. 8b suggested that the degradation percentage of TC obviously increased with the catalyst amount in the filter. This phenomenon is probably due to the augmentation of catalysts, which enhances the trajectory and complexity of the PMS and TC molecules as they traverse the filter. This prolongs the duration of contact between them and the catalyst. Consequently, this increase in contact time leads to an escalation in the activation rate of PMS and a concomitant enhancement in the degradation of TC. The findings indicate that CS@2Oat-N_U functions as a highly effective catalyst for the continuous dynamic treatment of wastewater.

Fig. 9. XPS spectra of CS@2Oat-N_U.

3.6. Catalytic mechanisms

To investigate the active site of the catalyst, XPS spectra of CS@2Oat-N_U were determined. As illustrated in Fig. S1, the major elements of the catalyst remained the same before and after five reactions, but their respective proportions exhibited a notable alteration. The relative proportions of C and N decreased from 60.4 % and 14.4 % to 57.5 % and 9.8 %, respectively, while the relative proportion of O increased from 25.2 % to 32.7 %. These findings indicate that elemental N was successfully doped into the carbon skeleton. In Fig. 9a and 9b, four peaks of C 1 s could be identified at approximately 284.2 eV, 284.8 eV, 285.7 eV, and 288.2 eV, which are attributed to C-C, C-O, C-N, and C=O functional groups, respectively [29,41]. After five cycles, the relative proportions of C-C, C-N and C=O decreased from 29.8 %, 22.3 %, and 20.4 % to 27.9 %, 16.4 %, and 12.3 %, respectively; while the proportion of C-O increased from 27.5 % to 43.4 %, which suggested that C-N and C=O functional groups are the potential active sites. As illustrated in Fig. 9c and d, four peaks of N 1 s were observed at 398.5 eV, 400.2 eV, 401.0 eV, and 404.9 eV, which are ascribed to pyridine N, pyrrole N, and graphitic N and oxidized N, respectively [42]. After five cycles, the relative proportions of pyridine N and graphite N decreased from 29.0 % and 30.7 % to 28.4 % and 27.6 %, respectively. Conversely, the relative proportions

of pyrrole N and oxidized N increased from 34.1 % and 6.2 % to 36.5 % and 7.5 %. These findings suggest that pyridine N, pyrrole N, graphite N, and oxidized N were involved in the reaction process simultaneously. Furthermore, it can be hypothesized that pyridine N and graphite N may represent active N species. In Fig. 9e and f, four peaks of O 1 s could be identified at 531.0 eV, 531.9 eV, 532.6 eV and 533.5 eV, which are attributed to C=O, O-C=O, C-O, and adsorbed H₂O, respectively [43,44]. After five cycles, the relative proportion of C=O decreased from 31.80 % to 22.38 %, while the relative proportion of O-C=O, C-O, and adsorbed H₂O increased from 18.97 %, 27.40 %, and 21.82 % to 22.90 %, 29.22 % and 23.66 %, respectively. The results presented above indicate the potential active sites of the catalyst were pyridine N, graphite N, C=O, and C-N functional groups.

To ascertain the ROSs in the CS@2Oat-N_U/PMS system, free radical quenching experiments were conducted. Methanol (MeOH), tertbutanol (TBA), *p*-benzoquinone (*p*-BQ), and furfuryl alcohol (FFA) are commonly used as scavengers for SO₄^{•-}, •OH, O₂^{•-} and ¹O₂, respectively. As illustrated in Fig. 10a and b, the presence of MeOH and TBA exhibited an inhibition effect on the degradation process, but this effect was limited. Even when the concentrations of MeOH and TBA were 0.6 M, the degradation percentage and k_{obs} of TC only declined to 78.65 %, 0.018 min⁻¹ and 82.35 %, 0.018 min⁻¹, respectively. This indicates that

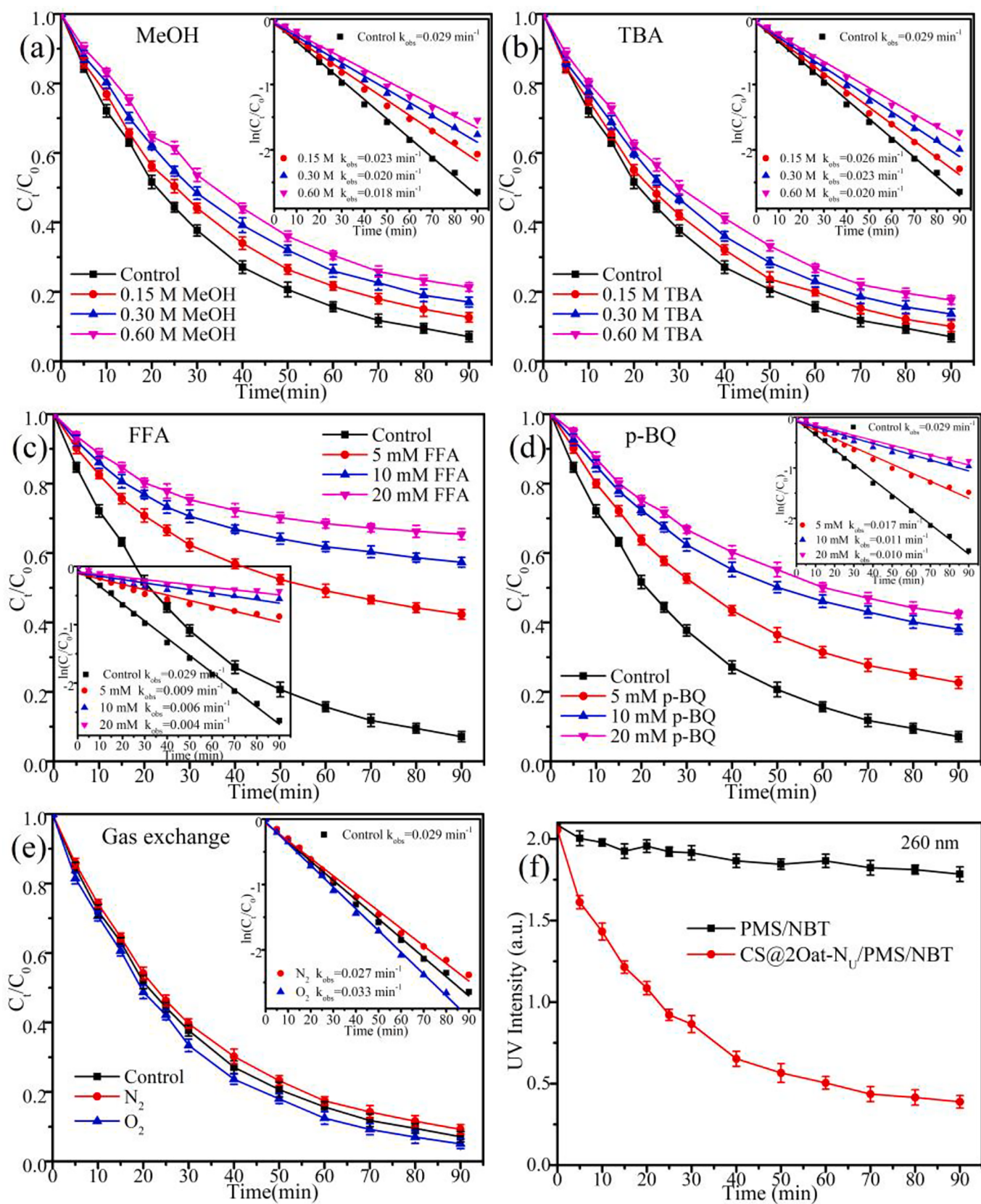


Fig. 10. Different quenching experiments (a-d). Gas exchange (e) and chemical probe (f) tests. Conditions: $[TC]_0 = 20 \text{ mg L}^{-1}$, $[CS@2Oat-N_U]_0 = 0.20 \text{ g L}^{-1}$, $[PMS]_0 = 0.10 \text{ g L}^{-1}$, pH = 3.68, T = 25 °C.

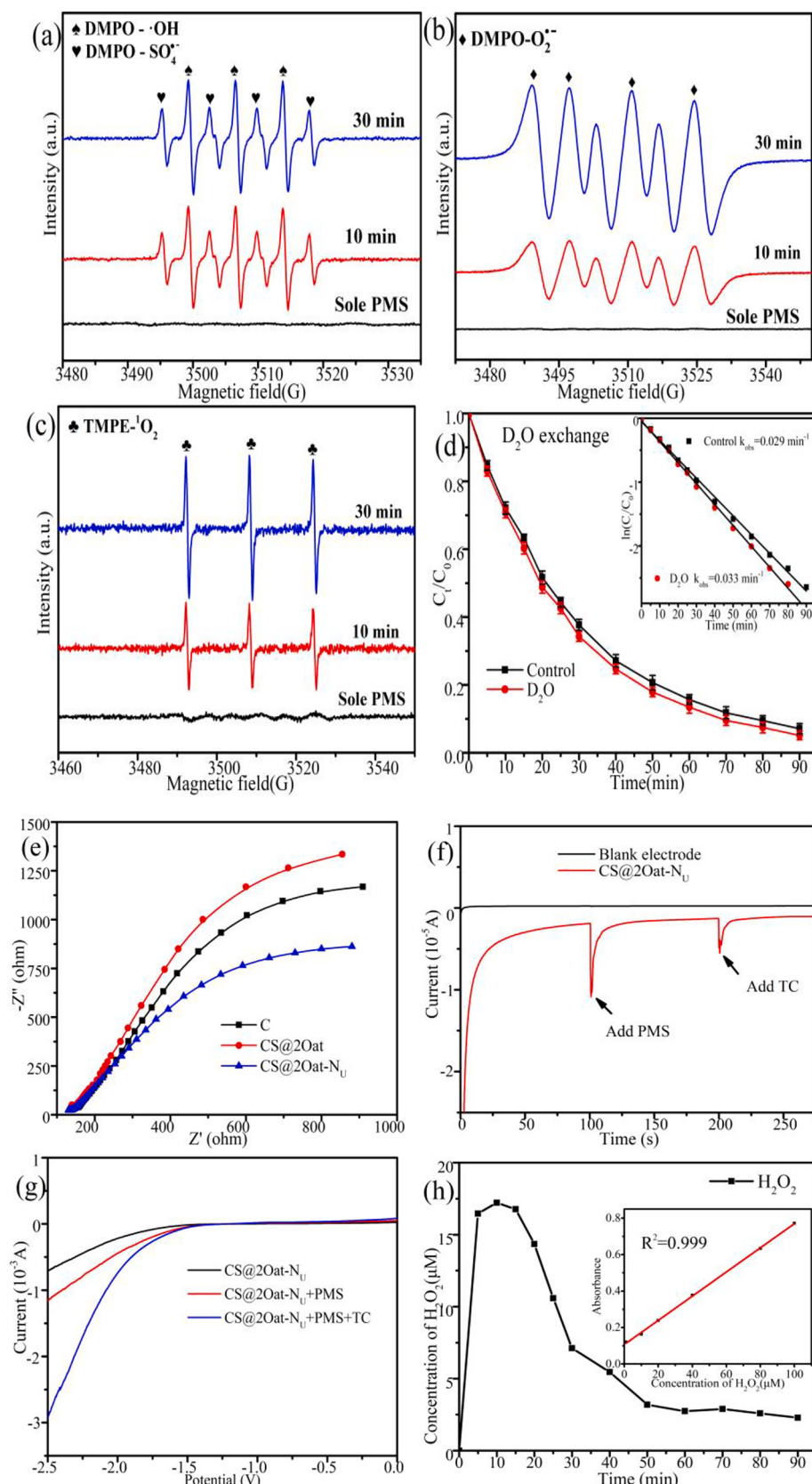


Fig. 11. EPR spectra (a-c), solvent exchange test (d), EIS (e), i-t cures(f), LSV (g) and H₂O₂ concentration (g). Conditions: [TC]₀ = 20 mg L⁻¹, [CS@2Oat-N_U]₀ = 0.20 g L⁻¹, [PMS]₀ = 0.10 g L⁻¹, pH = 3.68, T = 25 °C.

$\text{SO}_4^{\bullet-}$ and $\bullet\text{OH}$ were present, but did not play a dominant role in the reaction system [45]. When the addition of FFA was only 5 mM (Fig. 10c), the degradation efficiency and k_{obs} of TC rapidly decreased to 57.68 % and 0.009 min^{-1} , respectively. With the addition of 20 mM FFA, the inhibition effect was further enhanced, reducing the values to 34.58 % and 0.004 min^{-1} , indicating that ${}^1\text{O}_2$ plays an important role in the degradation of TC [46]. As depicted in Fig. 10d, the addition of 5 mM, 10 mM, and 20 mM of *p*-BQ also resulted in a notable decline in the degradation percentage and k_{obs} of TC, reaching 77.32 %, 61.99 %, 57.68 % and 0.017 min^{-1} , 0.011 min^{-1} , 0.01 min^{-1} , respectively. This observation suggests the presence of $\text{O}_2^{\bullet-}$ in the system. To further verify the presence of $\text{O}_2^{\bullet-}$, gas exchange experiments were conducted by continuously passing O_2 and N_2 into the reaction system. As illustrated in Fig. 10e, the degradation percentage and k_{obs} of TC exhibited a slight increase to 94.96 % and 0.033 min^{-1} with the injection of O_2 ; conversely, a decrease to 90.78 % and 0.027 min^{-1} was observed with the injection of N_2 , indicating the presence of $\text{O}_2^{\bullet-}$ and its participation in the degradation reaction [47]. Additionally, the chemical probe test based on nitroblue tetrazolium (NBT) as a free radical probe was conducted. As depicted in Fig. 10f, the CS@2Oat-N_U/PMS/NBT system exhibited a notable reduction in the absorbance value at 260 nm in comparison to the PMS/NBT system. This observation further corroborates the hypothesis that a considerable number of $\text{O}_2^{\bullet-}$ were indeed generated within the system.

To further determine the ROSs, EPR experiments were conducted using DMPO and TEMP as spin-trapping agents [48]. As illustrated in Fig. 11a to 11c, the EPR spectra exhibited no characteristic peaks when only PMS existed in the system, indicating that the ROSs generated by PMS alone were negligible. Following the simultaneous addition of the catalyst and PMS, the characteristic peaks of the signals for DMPO- $\bullet\text{OH}$, DMPO- $\text{SO}_4^{\bullet-}$, DMPO- $\text{O}_2^{\bullet-}$, and TEMP- ${}^1\text{O}_2$ were observed in the reaction system, respectively. Furthermore, the intensities of all peaks increased with the reaction time, indicating that $\text{SO}_4^{\bullet-}$, $\bullet\text{OH}$, $\text{O}_2^{\bullet-}$ and ${}^1\text{O}_2$ were produced in the system. However, it has been proposed that the inhibition of the degradation reaction by FFA may be due to the direct reaction between FFA and PMS rather than to the quenching of ${}^1\text{O}_2$ [49]. Furthermore, it has been suggested that the TEMP- ${}^1\text{O}_2$ signal may also result from electron transfer between TEMP and the catalyst/PMS system rather than from the actual capture of ${}^1\text{O}_2$. Given that the lifetime of ${}^1\text{O}_2$ in deuterioxide (D_2O) is longer (20–32 μs) than that in H_2O (2 μs), the degradation experiments were performed using D_2O as the solvent. As illustrated in Fig. 11d, the degradation percentage of TC in D_2O was marginally higher than that in H_2O , which suggests the presence of ${}^1\text{O}_2$ and its pivotal role in this system. The aforementioned results indicate that $\text{SO}_4^{\bullet-}$, $\bullet\text{OH}$, $\text{O}_2^{\bullet-}$, and ${}^1\text{O}_2$ were generated during the activation of PMS for TC degradation. Among these, the $\text{O}_2^{\bullet-}$ and ${}^1\text{O}_2$ were the dominant ROSs, which was consistent with the findings of the quenching experiments.

As the carbon-based catalyst could act as both an electron acceptor and electron donor for electron transfer during the degradation of organic pollutants, electrochemical techniques including electrochemical impedance spectroscopy (EIS), electric current curves (it), and linear sweep voltammetry (LSV) were conducted. As illustrated in Fig. 11e, the CS@2Oat-N_U exhibited a smaller semicircle diameter compared to C and CS@2Oat, indicating that CS@2Oat-N_U demonstrated a lower electron transfer resistance and a more rapid electron transfer capability. This suggested that the doping of urea enhanced the electron transfer performance. As illustrated in Fig. 11f, when the working electrode was a bare glassy carbon electrode, the current change was negligible up the addition of PMS and TC. However, significant current fluctuations were observed when glassy carbon electrodes were coated with the catalyst under the same conditions. The linear scanning voltammetry (LSV) curves (Fig. 11g) showed that the current gradually enhanced with the addition of PMS and TC, indicating that the generation of the ternary system facilitated the degradation process [50]. The results presented above demonstrate that electron

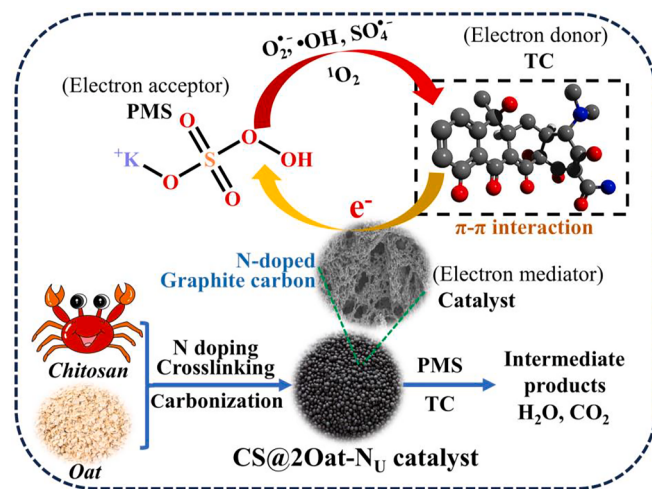
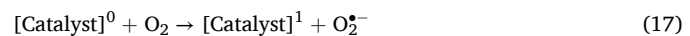
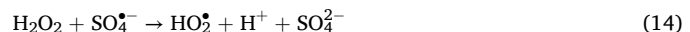
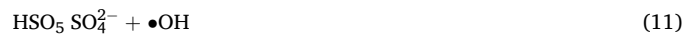
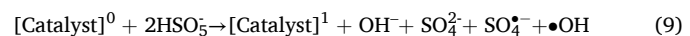


Fig. 12. Catalytic mechanism of CS@2Oat-N_U for TC degradation.

transfer indeed occurs between the catalyst, PMS, and TC molecules.

Based on the above conclusions, the radical and non-radical pathways of the system were verified, and a proposed catalytic mechanism was formulated in Fig. 12. (i) The CS@2Oat-N_U serves as an electronic mediator, facilitating electron transfer between CIP and PMS molecules by serving as a bridge. The abundant pore characteristics of CS@2Oat-N_U provide numerous adsorption sites for both PMS and CIP molecules in solution. Specifically, TC molecules are adsorbed onto the CS@2Oat-N_U surface via π - π interactions, whereas charge-transfer interactions also contribute to the adsorption of TC on the CS@2Oat-N_U surface. (ii) The activation of PMS molecules occurs via interaction with active sites on the CS@2Oat-N_U surface, including defective structures, C=O groups, and sp²-hybridized carbon, leading to the formation of $\bullet\text{OH}$ and $\text{SO}_4^{\bullet-}$. At the same time, graphitic nitrogen present on the CS@2Oat-N_U surface facilitates faster electron transfer between PMS and TC. Additionally, upon exposure to electrons, the O-O bond in PMS is cleaved, leading to the formation of SO_4^{2-} and H_2O_2 . (iii) The generated H_2O_2 quickly interacted with $\bullet\text{OH}$ and $\text{SO}_4^{\bullet-}$, resulting in the production of HO_2^{\bullet} . Subsequently, the formed HO_2^{\bullet} decomposed into $\text{O}_2^{\bullet-}$, which then reacted with PMS to produce ${}^1\text{O}_2$ [51]. To confirm this hypothesis, the concentration of H_2O_2 in the system was quantified. As illustrated in Fig. 11h, the concentration of H_2O_2 increased rapidly during the initial 20 min, followed by a gradual decline. This suggests that H_2O_2 was generated and consumed within the reaction system. In conclusion, the electron transfer-induced degradation of TC and the subsequent formation of ROSs led to the formation of small molecules, as well as non-toxic byproducts.



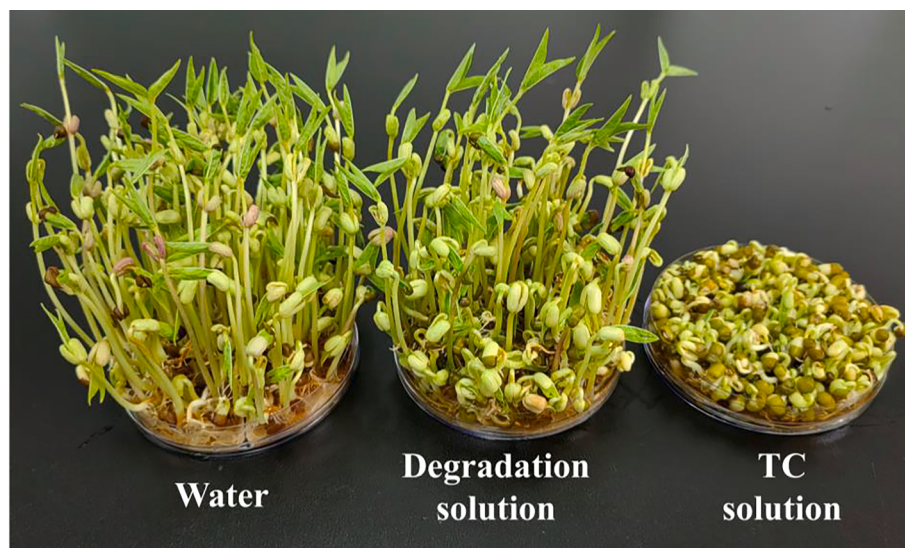


Fig. 13. Phenotype of representative mung beans treated by different solution.

3.7. Intermediate product analysis of TC degradation

The oxidation percentage of total organic carbon (TOC) is a pivotal reference factor in AOPs. Fig. S2 illustrates the TOC removal in the CS@2Oat-N_U/PMS system during the oxidation of TC. The results indicate that approximately 58.6 % of the organics are oxidized within 90 min, suggesting that the CS@2Oat-N_U/PMS system possesses a considerable capacity to convert TC into non-toxic CO₂, NH₄⁺, and H₂O.

Based on the intermediates identified by HPLC-MS (Fig.S3) and the findings of previous studies, three potential degradation pathways were postulated (Fig.S4). In pathway I, the TC was initially demethylated to yield IP1 (*m/z* = 449), which was then dehydroxylated to form IP2 (*m/z* = 417) [52]. In pathway II, the product IP3 (*m/z* = 417) was generated by N-dealkylation from TC, and then the product IP4 (*m/z* = 401) was generated by the dehydration pathway in the presence of PMS [53]. In pathway III, the –NC₂H₆ and –CONH₂ bonds of TC are preferentially broken to generate IP5 (*m/z* = 359), and IP5 was ring-opened to generate IP6 (*m/z* = 306) [54]. The intermediates IP2, IP4, and IP6 underwent a series of reactions, including ring opening and cleavage, to form the lower molecular weight compounds IP7 (*m/z* = 114), IP8 (*m/z* = 78), and IP9 (*m/z* = 122). Subsequently, the degradation of these small molecules produces water, carbon dioxide, and low molecular weight metabolites.

To evaluate the biotoxicity of TC and its degradation products, a germination experiment using mung beans was conducted as a means of validation. As shown in Fig. 13, the germination and growth rates of mung beans in the three distinct solutions exhibited notable disparities. As can be seen, the mung beans grew vigorously in deionized water, and the germination rate reached 100 %. Although the growth and germination of mung beans in the degraded TC solution catalyzed by CS@2Oat-NU were inferior to those observed in water, the growth rate and germination remained satisfactory. However, in the TC solution, nearly all of bean sprouts exhibited stunted growth, and the germination rate of mung beans was markedly reduced. The result evidence that the biotoxicity of TC can be effectively mitigated by the CS@2Oat-N_U/PMS system.

4. Conclusion

Environmentally-friendly 3D non-metallic spherical catalysts based on oats and chitosan were prepared via freeze-drying and pyrolysis. The spherical catalyst (CS@2Oat-N_U) exhibited excellent performance in activating PMS to degrade tetracycline (20 mg L⁻¹, 92.89 %) when the

mass ratio of chitosan to oats and carbonization temperature were 1:2 and 700 °C, respectively. Radical scavenger and EPR experiments demonstrated that O₂[•] and ¹O₂ were the primary agents responsible for TC degradation. XPS analysis revealed that the potential active sites for PMS activation were pyridine N, graphite N, and functional groups of C=O and C-N. Furthermore, cycling experiments and interference experiments demonstrated that CS@2Oat-N_U exhibited excellent stability and anti-interference performance. Seed germination experiments showed that the CS@2Oat-N_U/PMS system could effectively reduce the biotoxicity of TC. The findings of this study provided a novel strategy for reusing mildewed oats and have also yielded a promising catalyst for the activation of PMS for TC degradation.

Declaration of competing interest

The authors declare that they have no known competing financial interests or personal relationships that could have appeared to influence the work reported in this paper.

Acknowledgements

The authors acknowledge the National Natural Science Foundation of China (22278118, 22108065), the Natural Science Foundation project of Hubei (2024AFB967).

Appendix A. Supplementary data

Supplementary data to this article can be found online at <https://doi.org/10.1016/j.seppur.2025.132317>.

References

- [1] M.I. Hutchings, A.W. Truman, B. Wilkinson, *Antibiotics: past, present and future*, *Curr. Opin. Microbiol.* 51 (2019) 72–80.
- [2] J. Chen, R. Sun, C. Pan, Y. Sun, B. Mai, Q.X. Li, *Antibiotics and food safety in aquaculture*, *J. Agric. Food Chem.* 68 (43) (2020) 11908–11919.
- [3] Y. Dai, M. Liu, J. Li, S. Yang, Y. Sun, Q. Sun, W. Wang, L. Lu, K. Zhang, J. Xu, *A review on pollution situation and treatment methods of tetracycline in groundwater*, *Sep. Sci. Technol.* 55 (5) (2020) 1005–1021.
- [4] T.H. Grossman, *Tetracycline antibiotics and resistance*, *Cold Spring Harb. Perspect. Med.* 6 (4) (2016) a025387.
- [5] K. Zheng, L. Xiao, *Iron and nitrogen co-doped porous carbon derived from natural cellulose of wood activating peroxyxonosulfate for degradation of tetracycline: role of delignification and mechanisms*, *Int. J. Biol. Macromol.* 222 (2022) 2041–2053.

- [6] S. Harsha, I. Herath, C. Lin, S. Ch, Industrial waste-based adsorbents as a new trend for removal of water-borne emerging contaminants, *Environ. Pollut.* 123(140) (2023).
- [7] H. Zeghoud, L. Fryda, H. Djelal, A. Assadi, A. Kane, A comprehensive review of biochar in removal of organic pollutants from wastewater: characterization, toxicity, activation/functionalization and influencing treatment factors, *J. Water Process Eng.* 47 (2022) 102801.
- [8] K. Song, Y. Liu, A. Umar, H. Ma, H. Wang, Ultrasonic cavitation: tackling organic pollutants in wastewater, *Chemosphere* 141(024) (2023).
- [9] Y. Zhang, H. Zhang, J. Yao, Y. Song, W. Li, X. Xuan, Coordination tuning of Fe^{2+} ions concentration in Fe-doped black phosphorus-carbonized cotton fiber (Fe-BP-CCF) composites to regulate photocatalysis and peroxyomonosulfate (PMS) activation towards highly efficient degradation of organic pollutants, *Chem. Eng. J.* 483 (2024) 149326.
- [10] Z. Chen, Y. Lu, X. Liu, J. Li, Q. Liu, Novel magnetic catalysts for organic pollutant degradation via contact electro-catalysis, *Nano Energy* 108 (2023) 108198.
- [11] Y. Ding, X. Wang, L. Fu, X. Peng, C. Pan, Q. Mao, C. Wang, J. Yan, Nonradicals induced degradation of organic pollutants by peroxydisulfate (PDS) and peroxyomonosulfate (PMS): recent advances and perspective, *Sci. Total Environ.* 765 (2021) 142794.
- [12] C.T. Chekem, S. Chiron, J. Mancaux, G. Plantard, V. Goetz, Thermal activation of persulfates for wastewater depollution on pilot scale solar equipment, *Sol. Energy* 205 (2020) 372–379.
- [13] J. Liu, H.L. So, W. Chu, Degradation of 1-naphthylamine by a UV enhanced Fe^{2+} /peroxyomonosulfate system: a novel pH-dependent activation pathway, *Chem. Eng. J.* 443 (2022) 136299.
- [14] M. Kohantorabi, G. Moussavi, S. Giannakis, A review of the innovations in metal- and carbon-based catalysts explored for heterogeneous peroxyomonosulfate (PMS) activation, with focus on radical vs. non-radical degradation pathways of organic contaminants, *Chem. Eng. J.* 411 (2021) 127957.
- [15] B. Kakavandi, S. Alavi, F. Ghanbari, M. Ahmadi, Bisphenol A degradation by peroxyomonosulfate photo-activation coupled with carbon-based cobalt ferrite nanocomposite: performance, upgrading synergy and mechanistic pathway, *Chemosphere* 287 (2022) 132024.
- [16] J. Hou, T. Zhang, T. Jiang, X. Wu, Y. Zhang, M. Tahir, A. Hussain, M. Luo, J. Zou, X. Wang, Fast preparation of oxygen vacancy-rich 2D/2D bismuth oxyhalides-reduced graphene oxide composite with improved visible-light photocatalytic properties by solvent-free grinding, *J. Clean. Prod.* 328 (2021) 129651.
- [17] D. Paudel, B. Dhungana, M. Caffe, P. Krishnan, A review of health-beneficial properties of oats, *Foods* 10 (11) (2021) 2591.
- [18] I. Jokinen, P. Silventoinen-Veijalainen, M. Lille, E. Nordlund, U. Holopainen-Mantila, Variability of carbohydrate composition and pasting properties of oat flakes and oat flours produced by industrial oat milling process—Comparison to non-heat-treated oat flours, *Food Chem.* 405 (2023) 134902.
- [19] F. Hu, Y. Liu, X. Shi, L. Xiao, Removal of organic contaminants by starch-derived porous carbon via peroxyomonosulfate activation: the role of N doping and Fe/Mn loading, *Colloids Surf. A Physicochem. Eng. Asp* 649 (2022) 129520.
- [20] Z. Zhou, Y. Bu, X. Long, J. Cai, N-containing biochar from oatmeal: hydrothermal synthesis and used as highly efficient adsorbent for Cr (VI) adsorptive-reduction removal, *Biomass Convers. Biorefin.* (2023) 1–10.
- [21] D. Yan, C. Yu, X. Zhang, W. Qin, T. Lu, B. Hu, H. Li, L. Pan, Nitrogen-doped carbon microspheres derived from oatmeal as high capacity and superior long life anode material for sodium ion battery, *Electrochim. Acta* 191 (2016) 385–391.
- [22] C. Liu, G. Zhang, H. Zhang, J. Zhao, Y. Wang, F. Jia, S. Song, Construction of Ag/MoS₂@Fe-CS aerogel as excellent PMS activator via synergistic photocatalysis and photothermal effects, *Chem. Eng. J.* 455 (2023) 140814.
- [23] J.-W. Tu, Y. Li, L. Chen, W. Miao, Iron-loading N and S heteroatom doped porous carbon derived from chitosan and CdS-Tetrahymena thermophila for peroxyomonosulfate activation, *Int. J. Biol. Macromol.* 253 (2023) 127347.
- [24] G.A. Kifle, Y. Huang, M. Xiang, T. Tesfamichael, W. Wang, Y. Wei, C. Wang, C. Li, H. Li, Synergistic enhancement of peroxyomonosulfate activation by bimetallic (Bi, Fe) supported NaHCO₃ activated and urea-modified biochar for sulfamethoxazole degradation: DFT calculations, toxicity assessments, and mechanistic studies, *J. Environ. Chem. Eng.* 12 (2) (2024) 111675.
- [25] W. Tian, H. Sun, X. Duan, H. Zhang, Y. Ren, S. Wang, Biomass-derived functional porous carbons for adsorption and catalytic degradation of binary micropollutants in water, *J. Hazard. Mater.* 389 (2020) 121881.
- [26] L. Jing, M. Xie, Y. Xu, C. Tong, X. Du, H. Zhao, N. Zhong, H. Li, J. Hu, Advanced oxidation via the synergy of C-defective/C-O band modified ultrathin porous g-C₃N₄ and PMS for efficient photothermal degradation of bisphenol pollutants and lignin derivatives, *Green Energy Environ.* 9 (7) (2024) 1159–1170.
- [27] X. Zhang, Y. Yang, H.H. Ngo, W. Guo, F. Sun, X. Wang, J. Zhang, T. Long, Urea removal in reclaimed water used for ultrapure water production by spent coffee biochar/granular activated carbon activating peroxyomonosulfate and peroxydisulfate, *Bioresour. Technol.* 343 (2022) 126062.
- [28] M. Tian, X. Ren, S. Ding, N. Fu, Y. Wei, Z. Yang, X. Yao, Effective degradation of phenol by activating PMS with bimetallic Mo and Ni Co-doped g-C₃N₄ composite catalyst: A Fenton-like degradation process promoted by non-free radical O_2^- , *Environ. Res.* 243 (2024) 117848.
- [29] Q. Shentu, Z. Wu, W. Song, S. Pan, Z. Zhou, W. Lv, C. Song, Y. Yao, Carbon doped boron nitride nanosheet as efficient metal-free catalyst for peroxyomonosulfate activation: Important role of BNC moieties, *Chem. Eng. J.* 446 (2022) 137274.
- [30] H. Jiang, Y. Duan, H. Li, A. Wang, New insight into highly efficient removal of tetracycline by calcined hydroxyapatite activated peroxyomonosulfate: the role of calcium carbonate and phosphate group, *J. Water Process Eng.* 55 (2023) 104207.
- [31] H. Zhang, S. Chen, L. Ran, H. Yu, Enhanced PMS activation by surface electronic reconstruction at Co₃O₄/ZnO heterointerface: Performance and mechanism, *Process Saf. Environ. Prot.* 171 (2023) 330–340.
- [32] K. Wang, P. Xiang, R. Zhou, M. Huang, P. Lin, Performance and mechanism of antibiotic removal by MOF-on-MOF-derived cobalt and nitrogen-doped magnetic porous carbon activated PMS, *J. Water Process Eng.* 54 (2023) 104043.
- [33] S. Yang, W. Zhang, M. Liu, H. Zhao, H. Lu, H. Li, Z. Guo, A. Yuan, J. Yang, J. Pan, Integrating built-in fine alloying FeNi₃ in carbon nanofiber reinforcing intermetallic synergy for PMS activation to degrade Bisphenol A, *J. Environ. Chem. Eng.* 11 (1) (2023) 109190.
- [34] S. Liu, Z. Zhang, F. Huang, Y. Liu, L. Feng, J. Jiang, L. Zhang, F. Qi, C. Liu, Carbonized polyaniline activated peroxyomonosulfate (PMS) for phenol degradation: role of PMS adsorption and singlet oxygen generation, *Appl. Catal. B* 286 (2021) 119921.
- [35] V.C. Dang, D.T. Tran, A.T. Phan, N.K. Pham, Synergistic effect for the degradation of tetracycline by rGO-Co₃O₄ assisted persulfate activation, *J. Phys. Chem. Solid* 153 (2021) 110005.
- [36] F. Ghanbari, M. Moradi, Application of peroxyomonosulfate and its activation methods for degradation of environmental organic pollutants, *Chem. Eng. J.* 310 (2017) 41–62.
- [37] Y. Feng, M. Liu, Q. Shi, Y. Song, L. Yang, J. Zhang, Z. Li, W. Zhu, Sludge-derived biochar applied in peroxyomonosulfate (PMS) activation: reactive oxygen species (ROS) dominated process and characteristics, *J. Environ. Chem. Eng.* 11 (6) (2023) 111365.
- [38] B. He, L. Song, Z. Zhao, W. Liu, Y. Zhou, J. Shang, X. Cheng, CuFe₂O₄/CuO magnetic nano-composite activates PMS to remove ciprofloxacin: ecotoxicity and DFT calculation, *Chem. Eng. J.* 446 (2022) 137183.
- [39] S. Yu, Y. Gao, R. Khan, P. Liang, X. Zhang, X. Huang, Electrosprayed PAN-based graphene/SnO₂ carbon nanofibers as anodic electrocatalysis microfiltration membrane for sulfamethoxazole degradation, *J. Membr. Sci.* 614 (2020) 118368.
- [40] X. Li, T. Chen, Y. Qiu, Z. Zhu, H. Zhang, D. Yin, Magnetic dual Z-scheme g-C₃N₄/BiVO₄/CuFe₂O₄ heterojunction as an efficient visible-light-driven peroxyomonosulfate activator for levofloxacin degradation, *Chem. Eng. J.* 452 (2023) 139659.
- [41] R.A.K. Hirani, A.H. Asif, N. Rafique, H. Wu, L. Shi, S. Zhang, X. Duan, S. Wang, M. Saunders, H. Sun, Three-dimensional nitrogen-doped graphene oxide beads for catalytic degradation of aqueous pollutants, *Chem. Eng. J.* 446 (2022) 137042.
- [42] G. Wang, Y. Liu, X. Dong, X. Zhang, Transforming radical to non-radical pathway in peroxyomonosulfate activation on nitrogen doped carbon sphere for enhanced removal of organic pollutants: combined effect of nitrogen species and carbon structure, *J. Hazard. Mater.* 437 (2022) 129357.
- [43] Y. Zeng, G. Zhou, D. He, G. Peng, Catalytic degradation of ciprofloxacin in aqueous solution by peroxyomonosulfate activated with a magnetic CuFe₂O₄@biochar composite, *Int. J. Mol. Sci.* 24 (6) (2023) 5702.
- [44] M. Li, D. Li, S. Li, J. Liu, H. Deng, D. Xia, Novel sludge-sugarcane bagasse mixed biochar as an efficient activator for peroxyomonosulfate to degrade bisphenol AF, *Chem. Eng. J.* 462 (2023) 142114.
- [45] P. Yang, A. Shen, Z. Zhu, L. Wang, R. Tang, K. Yang, M. Chen, H. Dai, X. Zhou, Construction of carbon nitride-based heterojunction as photocatalyst for peroxyomonosulfate activation: Important role of carbon dots in enhancing photocatalytic activity, *Chem. Eng. J.* 464 (2023) 142724.
- [46] Q. Zhao, W. Yin, M.T. Sarwar, C. Gao, K. Yuan, H. Yang, Thermal annealing-enhanced interfacial charge transfer in g-C₃N₄/reectorite composite for boosted peroxyomonosulfate activation, *J. Environ. Chem. Eng.* 11 (2) (2023) 109491.
- [47] X. Zhou, H. Luo, B. Sheng, X. Chen, Y. Wang, Q. Chen, J. Zhou, $\text{Cu}^{2+}/\text{Cu}^+$ cycle promoted PMS decomposition with the assistance of Mo for the degradation of organic pollutant, *J. Hazard. Mater.* 411 (2021) 125050.
- [48] W. Lu, L. Qi, D. Dong, X. Shen, L. Xu, Y. Zhang, X. Mei, W. Qiao, X. Guo, Y. Pan, A comparison study of photocatalytic performance of g-C₃N₄ prepared from different precursors for the activation of different peroxides, *Sep. Purif. Technol.* 327 (2023) 124904.
- [49] Y. Long, Y. Huang, H. Wu, X. Shi, L. Xiao, Peroxyomonosulfate activation for pollutants degradation by Fe-N-codoped carbonaceous catalyst: structure-dependent performance and mechanism insight, *Chem. Eng. J.* 369 (2019) 542–552.
- [50] S. Zuo, D. Li, F. Yang, H. Xu, M. Huang, Z. Guan, D. Xia, Copper oxide/graphitic carbon nitride composite for bisphenol A degradation by boosted peroxyomonosulfate activation: mechanism of Cu-O covalency governs, *J. Colloid Interface Sci.* 603 (2021) 85–93.
- [51] W. Peng, J. Liao, Y. Yan, L. Chen, C. Ge, S. Lin, Enriched nitrogen-doped carbon derived from expired drug with dual active sites as effective peroxyomonosulfate activator: ultra-fast sulfamethoxazole degradation and mechanism insight, *Chem. Eng. J.* 446 (2022) 137407.
- [52] G. Zhou, S. Wen, J. Wang, X. Zhou, Y. Xu, Y. Guan, F. Zhu, J. Yin, C. Liu, L. Zhang, Shorter migration distance of ROS and accelerate electron transfer by engineering dual Lewis acid sites for synergistic activation of PMS toward rapid TC degradation, *Sep. Purif. Technol.* 330 (2024) 125244.
- [53] X. Peng, Z. Yang, P. Zhan, Y. Chai, Z. Ning, F. Hu, H. Dai, Construction of core-shell Fe₃O₄@MoS₂ activates peroxyomonosulfate for the degradation of tetracycline: structure-activity relationship, performance and mechanisms, *J. Alloy. Compd.* 961 (2023) 170991.
- [54] H. Cheng, H. Liu, C. Huang, J. Xu, H. Tian, J. Yang, P. Wang, J. Cai, M. Cheng, Z. Liu, Tungsten carbide induced acceleration of $\text{Fe}^{3+}/\text{Fe}^{2+}$ cycle in $\text{Fe}^{2+}/\text{PMS}$ process for rapid degradation of tetracycline hydrochloride, *Sep. Purif. Technol.* 330 (2024) 125311.